INSTITUTE OF PLASMA PHYSICS

NAGOYA UNIVERSITY

ABNORMAL ENERGY DEPOSITION ON THE WALL THROUGH PLASMA DISRUPTIONS

K. Yamazaki and G. L. Schmidt

(Received – June 14, 1984)

IPPJ- 684 July 1984

RESEARCH REPORT

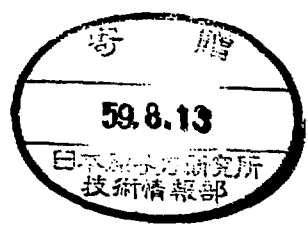

NAGOYA, JAPAN

ABNORMAL ENERGY DEPOSITION ON THE WALL THROUGH PLASMA DISRUPTIONS

K. Yamazaki and G. L. Schmidt*

(Received - June 14, 1984)

IPPJ - 684 July 1984

Presented at
Sixth International Conference on
Plasma Surface Interactions in Controlled Fusion Devices,
Nagoya University, Nagoya JAPAN,
May 14-18, 1984

Further communication about this report is to be sent to the Research Information Center, Institute of Plasma Physics, Nagoya University, Nagoya 464, Japan.

---

* Plasma Physics Laboratory, Princeton University, Princeton, NJ 08544, U.S.A.

ABSTRACT

The dissipation of plasma kinetic and magnetic energy during sawtooth oscillstions and disruptions in tokamaks is analyzed using Kadomtsev's disruption model and the plasma-circuit equations. New simple scalings of several characteristic times are obtained for sawteeth and for thermal and magnetic energy quenches of disruptions. The abnormal energy deposition on the wall during major or minor disruptions, estimated from this analysis, is compared with bolometric measurements in the PDX tokamak. Especially, magnetic energy dissipation during current termination period is shown to be reduced by the strong coupling of the plasma current with external circuits. These analyses are found to be useful to predict the phenomenological behavior of plasma disruptions in large future tokamaks, and to estimate abnormal heat deposition on the wall during plasma disruptions.

1. INTRODUCTION

Plasma disruptions in tokamaks is one of key problems to be solved for the steady-state reactors with tolerable thermal and mechanical loading on the wall and the structural materials. At present, the behavior of disruptions in tokamaks is clarified only qualitatively [1] . From the view-point of the design of large tokamak devices, it is important to predict the energy deposition on the wall during disruptions, as well as to find out an effective way of controlling disruptions.

The expected wall heat loads during normal operations and disruptions have been reviewed in Ref [2] . The increased wall heat load caused by sawtooth oscillations at high-$q_{surface}$ is usually neglected. However significant increases in pyroelectric signals are observed in PDX in the presence of large sawteeth at low-$q_{surface}$ and during fishbone oscillations. These increases are correlated with sawtooth drop or fishbone burst and may represent enhanced charge-exchange losses paticularly in the case of fishbone oscillations.

As for major disruptions, dangerous effects of thermal and mechanical damages on the wall and structural materials should be taken into account. During thermal quench period, most of plasma kinetic energy is dissipated to the limiter and the vacuum vessel. On the other hand, plasma magnetic energy, which is related to the plasma current and is generally larger than the plasma kinetic energy, may be dissipated during current quench period. larger than the plasma kinetic energy.

The total "energy" associated with these dissipations can be roughly estimated form the plasma current and the plasma poloidal beta values, while the maximum heat "power" loss to the material surface depends strongly on the characteristic time of disruptions and the spatial distribution of the energy deposition.

In this paper, temporal and spatial distributions of the disruption-induced heat load in tokamaks are outlined. As for internal disruptions, a simple scaling of sawtooth period is obtained by using Kadomtsev's disruption model. Some scalings of the time constant related to major disruptions are derived from a plasma-circuit model with simple energy balance equations. The estimated wall heat load is compared with the results obtained by bolometric measurements on PDX.

2. EXPERIMENTAL ARRANGEMENT

The bolometric measurement during major disruption in the PDX tokamak has been already reported in Ref. [3] , emphasizing the dissipation of the magnetic energy. Thermistor and pyroelectric detectors have been used to measure wall loss power in the forms of radiation and charge-exchange neutrals. A 19 channel themistor array with a response time of approximately 20 ms [4] , has been used to measure the poloidal symmetry of these energy losses and to calculate the total energy loss during a disruption. The toroidal symmetry has been checked by two separate single channel $LiTaO_3$ pyroelectric detectors; one is near the limiter and the other at 90 ° from the limiter. The temporal variation of the disruptive power loss has been

checked by a single-channel free standing thermistor with the response time of approximately 1 ms and the pyroelectric detectors having a response time of $\sim$ 200 μ sec. The measurements discussed here were focused on the modulation of pyro-electric signals and on the total radiated energy loss due to sawteeth, fishbone oscillations and disruptions.

3. SAWTEETH AND FISHBONE OSCILLATIONS

Previous theoretical and empirical estimates for sawtooth period have been reported in Refs. [5-8] . Here, we estimate the characteristic period of sawteeth and fishbone oscillations, using the magnetic reconnection model with parabolic current profile proposed by B. B. Kadomtsev [9] , and combining the field diffusion equation, the simplified temperature equation in the plasma center;

$$\partial T_e(t,0)/\partial t = T_e(t,0)/\tau_{heat}$$

and the equation of the temperature on the singular surface ($r = r_s$);

$$\partial T_e(t,r_s)/\partial t = 0 ,$$

we obtain the perturbed q^{-1}-profile and Te-profile;

$$\Delta q^{-1} = (\Delta_j/8)[(3t/\tau_{saw} + 5t^2/\tau_{saw}^2) - 2 (1+3t/\tau_{saw})(r/r_s)^2] \quad (1)$$

and

$$\Delta Te = (1-(r/r_s)^2) (t/\Delta_{heat} - (\Delta_j/16) (\tau_{skin}/\tau_{saw}) (r/r_s)^2) \quad (2)$$

where τ_{skin} and τ_{heat} are the skin and heating times defined with regard to the singular radius ($r = r_s$), and Δ_j is the current density perturbation on the plasma axis. Using the energy conservation within the mixing zone of radius $\sqrt{2}\, r_s$, we can obtain the semi-empirical

scaling for sawtooth oscillations [8]

$$\tau_{saw} = \sqrt{5\Delta_j/24}\,\tau_{heat}^{1/2}\,\tau_{skin}^{1/2} \sim (\sqrt{\lambda}/3)(r_s/a)\,\tau_{heat}^{1/2}\,\tau_{skin}^{1/2} \qquad (3)$$

where the following current density profile before disruptions is assumed;

$$j \propto 1 + \Delta_j(1-2(r/r_s)^2) \quad (\text{for } r < \sqrt{2}\,r_s)$$
$$\propto (1 - (r/a)^2)^{\lambda} \quad (\text{for } r > \sqrt{2}\,r_s).$$

then,

$$\Delta_j \sim (\lambda/2)(r_s/a)^2 .$$

The heat power loss from the plasma core to the region outside the q = 1 surface due to internal disruptions [9] is estimated from

$$P_{loss} = (\Delta W_e(t=\tau_{saw}) - \Delta W_e(t=0))\,V(r=r_s)/\tau_{saw}$$
$$\sim (1/4)(r_s/a)^2\,P_{loss}^{total}$$

which cannot be neglected when the q=1 radius is comparable to the plasma radius a_p, namely low-q operations. The auxiliary heating leads to the large 'inverse' sawteeth on the pyro-electric detector as shown in Fig. 1.(a). The radial profile of the bolometric signal is usually flat or hollow, therefore the normal sawtooth pattern could not be seen on the pyroelectric signals. In this two-beam case, the inverse-sawtooth amplitude is 20 ~ 30 % of the averaged pyro-electric signal.

The modulation in the pyro-electric signal during fishbone instabilities becomes more significant than that during sawtooth oscillations. This may be due to tne fact that during fishbone oscillations the dominant component of the energy loss is charge-exchange neutrals from nearly perpendicularly injected high energy particles [10] . Because of its geometry, the pyro-electric

signal is particularly sensitive to these losses. The pyro-electric signal related to fishbone instabilities in PDX tokamak is shown in Fig. 1.(b). The peak of the pyro-electric signal coincides with the amplitude of Mirnov signals, charge-exchange neutral signals and H_α intensities. The averaged bolometric signal during neutral beam operations (giant sawteeth (2 MW < P_{beam}< 5 MW) and fishbone cycles (6 MW < P_{beam})) is almost linearly proportional to the input power of NBI heating, whereas, the maximum pyro-electric signal during fishbone fluctuations is almost two times larger than the average power loss, as shown in Fig. 2.

4. MAJOR DISRUPTIONS

(4.-1.) Observations in PDX

During major disruptions, abnormal radiation losses are observed as shown in Fig.3 obtained in PDX. The total energy included in the plasma could be released completely during major disruptions, which is divided into two kinds of energy; the plasma kinetic energy W^{kin} and the magnetic energy W^{mag} (Fig.4). Schematically, the kinetic energy is supposed to be lost mainly near the limiter surface during thermal quench period and the magnetic energy associated with the plasma current is lost to the wall in the form of radiation and charge-exchange neutrals during the current termination.

As far as the bolometric measurement on PDX is concerned [3], the poloidal asymmetries before and after disruptions are not significant. For the toroidal symmetry, the bolometric energy loss

near the limiter is 1.5 ~ 2 times larger than that away from the limiter, while the ratio of these two is essentially unchanged during the disruption.

In addition to bolometric results, the measuremed temperature rise on the limiter surface due to local heat deposition should be paid attention and has been discussed on TFR [11] , D-III [12] and PDX [13] . Completely different heat deposition patterns during the disruption from that of non-disruptive discharge have been reported.

(4.-2.) Plasma-Circuit Model Relevant to Major Disruptions

The thermal energy quench during major current disruptions is characterized by the quick decay of the plasma temperature and significant inward shift of the plasma column, while the plasma current increases a little and the plasma density keeps almost constant. On the other hand, the magnetic energy quench is associated with the decay of total plasma current, the characteristic time of which depends strongly on the coupling of the plasma current to the external circuit. By using the plasma-circuit model with plasma energy balance, the behavior of post-disruptive plasma can be described [3, 14] .

We can write the momentum and energy equations of the plasma column, and circuit equations for plasma and coils;

$$d(mdR/dt)/dt = \partial \left((1/2)L_p^* I_p^2 + \sum_{j \neq p} M_{pj} I_p I_j \right) / \partial R \qquad (5)$$

$$d(3nTV)/dt = P_{beam} + R_p I_p^2 - 3nTV/\tau_E \qquad (6)$$

$$d(L_p I_p)/dt + R_p I_p = - d(\sum_{i \neq p} M_{pi} I_i)/dt = V_{loop} \qquad (7)$$

$$L_i dI_i/dt + R_i I_i + \sum_{j \neq i} M_{ij} dI_j/dt + d(M_{ip} I_p)/dt = V_i \ .$$

(for $i \neq p$) (8)

where R, m, V, R_p and I_p denote major radius, total mass, total volume, resistance and toroidal current of the plasma column, respectively. L_i, R_i and V_i are self-inductance, resistance and external power-supply voltage of the i-th external coil, respectively. The simple case with plasma, vertical field and vacuum vessel is described by

$$m(d^2R/dt^2) = -2\pi R I_p B_v + (\mu_o/2) I_p^2 (\ln(8R/a) + \Lambda - 1.5) + \partial (M_{ps} I_p I_s)/\partial R \quad (5a)$$

$$3nd(TV)/dt = P_{beam} + R_p I_p^2 - 3nTV/\tau_E \quad (6a)$$

$$d(L_p I_p)/dt + R_p I_p + d(M_{ps} I_s)/dt + d(\pi R^2 B_v)/dt = 0 \quad (7a)$$

$$L_s d(I_s)/dt + R_s I_s + I_p(\partial M_{sp}/\partial R)(dR/dt) + M_{sp}(dI_p/dt) = 0 \quad (8a)$$

(4.-2.-1.) Thermal Quench Model

During the thermal quench period, changes in the total plasma current and the plasma density can be neglected, and this quench time is estimated by Eqs. (6a) and (7a) with the simple confinement scaling for magnetic island width Δ [1]

$$\tau_{tq} = (a/\Delta)^2 qR/v_{th} \propto qR/\sqrt{T} \quad (9)$$

then, combining with Eq. (6a)

$$dT/dt \propto T^{3/2} .$$

The plasma temperature and hence the poloidal beta value decay parabolically in time,

$$T \propto (1+(t/t_{1/4}))^{-2},$$

where $t_{1/4}$ is the characteristic time for temperature to decrease to the 1/4 of the temperature prior to the disruption.

The reduction of poloidal beat, $\Delta\Lambda$, leads to the inward shift of the

plasma column, which is derived by linearizing Eq.(5a):

$$R \rightarrow R + \Delta R$$

$$B_v \rightarrow B_v + \Delta R(\partial B_v/\partial R)$$

$$\Lambda \rightarrow \Lambda + \Delta\Lambda$$

and

$$I_s \rightarrow \Delta I_s$$

Then,

$$\Delta R/R = \Delta\Lambda/ [(1-n)(\ln(8R/a)-1.5+\Lambda) - 1 + (R/a)(\Delta a/\Delta R) - (2/\mu_0)(\partial M_{ps}/\partial R)/L_s)(\tau_s/\tau)] \quad (10)$$

where n, τ_s and τ denote the vertical field curvature index, the L/R time of the shell and the growth time of this movement. The last two terms in the denominator means stabilizing effects due to the existence of the vessel and to the reduction of the plasma minor radius. This formula covers the results of M.Okabayashi et al. [15] . The poloidal flux conserving condition, $L_pI_p \propto L_p \sim$ const., gives rise to the relation $R\Delta a/a\Delta R \sim 1$. When the minor radius is determined by the geometrical limit, this term $R\Delta a/a\Delta R \sim R/a$ works more effective than that in the limiter-free flux-conserving case.

(4.-2.-2.) Magnetic Quench Model

The simple estimation [16] of the plasma current decay period is given by

$$\tau_{mq} \sim L_{eff}/R_{eff} \quad (11)$$

where effective inductance and resistance are

$$L_{eff} = L_p - M_{pc}^2/L_p ,$$

and

$$R_{eff} = R_p + R_c \quad ,$$

respectively, and the plasma temperature is assumed almost constant. Here M_{pc} is mutual inductance between the plasma and the external circuit. As pointed out in Ref [1] , including temperature decrease, the decay of the plasma current is linear in time

$$dI_p/dt \propto (n/qR)^{1/2} \qquad (12)$$

which is derived from Eqs. (6 ~ 8) and the confinement scaling such as Eq. (9). The temporal variation of various parameters can be schematically written as

$$I_p \propto 1-t/t_o$$

$$T_e \propto I_p^{2/3} \propto (1-t/t_o)^{2/3}$$

$$W_{loss}^{mag} \propto (2-t/t_o)(t/t_o)$$

and

$$P_{loss} \propto 1-t/t_o$$

where t_o is the current decay time, as illustrated in Fig. 4, which qualitatively coinsides with the typical PDX result in Fig. 3. The scaling of the current decay time is therefore obtained combining Eq.(12) with the Murakami density scaling $n \sim B_T/R$,

$$\tau_{mq} \propto (I_p V)^{-1/2} \qquad (13)$$

The tendency of the increase in the current decay time for higher current and larger volume devices is confirmed in Table 1 and Fig. 5, using data referred in Ref. [17] .

The energy deposition on the wall during disruptions is analyzed integrating Eqs (1-4) directly [3] , with measured plasma current, position and each circuit current. The energy loss during the disruption can be roughly estimated from the magnetic self-inductive energy of the plasma current, $(1/2)L_pI_p^2$. However, it was shown by

this calculation that the coupling $\sum_{j\neq p} M_{pj}I_pI_j$ of the plasma current to the other circuits reduced the actual loss to 3/4 of this rough estimation. From non-disruptive discharges the measured bolometric loss accounts for 1/3 of ΔW^{loss} estimated by the model, while the measured bolometric loss during disruptions corresponds to 80 $\sim$ 100 % of the calculated loss independent of the rate of disruptive current terminations.

5. SUMMARY

The characteristics of the pyro-electric signal of sawtooth and fishbone oscillations on PDX are discussed based on the bolometric measurements. Beam-heating-induced giant inverse-sawteeth are observed which increase the detected signal level 20 $\sim$ 30 % higher than that observed in no-sawtooth cases. High power perpendicular injection induces fishbone oscillations which double or triple the observed peak signal level above that of no-fishbone discharges. These large modulations are likely caused by the beam charge-exchange losses. The analyses related to internal disruptions are done using Kadomtsev's model and simple temperature relaxation model. Then the simple new scalings for sawtooth period and heat power loss are obtained and compared with several experiments.

The energy dissipation during the major disruption is measured bolometrically and analyzed using plasma-circuit model with plasma energy balance. The measurements show that the magnetic energy dissipated during current disruptions is lost by radiation and

charge-exchange uniformly to the wall. This magnetic energy dissipation might be reduced by providing circuits strongly coupled to the plasma current, which could be switched on at the time of the disruption using negative voltage spike as a trigger. By this means, the magnetic energy dissipated to the plasma might be reduced to that associated only with the plasma internal inductance.

ACKNOWLEDGEMENTS

The authors wish to thank Drs. K.Bol, K.McGuire and M.Okabayashi for stimulating discussions. Especially, fruitful comments on fishbone oscillations and disruptions were obtained from Dr. K.McGuire.

REFERENCES

[1] B.B.Kadomtsev, Plasma Phys. Controlled Fusion 26 (1984) 271.

[2] H.Vernickel, J. Nucl. Mater. 111 & 112 (1982) 531.

[3] K.Yamazaki and G.L.Schmidt, Nucl. Fusion 24 (1984) 467 ; IPPJ-644 (1983).

[4] J.Schivell, G.Renda, J.Lowrance and H.Hsuan, Rev.Sci.Instrum. 53 (1982) 1527.

[5] B.V.Waddell, G.L.Jahns, J.D.Callen and H.R.Hicks, Nicl. Fusion 18 (1978) 735.

[6] K.McGuire and D.C.Robinson, Nucl.Fusion 19 (1979) 505.

[7] Equipe TFR, Nucl. Fusion 20 (1980) 1227.

[8] K.Yamazaki, K.McGuire and M.Okabayashi, PPPL-1840 (1982).

[9] B.B.Kadomtsev, Fizika Plasmy 1 (1975) 710 [Sov. J. Plasma Phys. 1 (1977) 389] .

[10] K.McGuire, R.Goldston, M.Bell, M.Bitter, K.Bol et al., Phys. Rev. Lett. 50 (1983) 891.

[11] TFR Group, EUR-CEA-FC-1114(1981).

[12] T.Taylor, N.Brooks and K.Ioki, J.Nucl. Mater., 111&112 (1982) 569.

[13] M.Ulrickson and H.W.Kugel, Nucl. Tech./Fusion4 (1983) 141.

[14] J.G.Murray and G.Bronner, PPPL-1910 (1982)

[15] M.Okabayashi, H.Maeda, H.Takahashi and M.Reusch, Nucl. Fusion 21 (1981) 271.

[16] TFR Group, EUR-CEA-FC-1151(1982).

[17] a) JET : K.J.Dietz, D.Bartlett, G.Baumel et al.

' Start-Up and Initial Operation of JET ' This Conference.

b) TFTR : K.McGuire, Private Communication; K.M.Young et al., Plasma Phys. 26 (1984) 11.

c) PLT, PDX, D-III, ISX-B, ALCATOR-A & C, T-10, TOSCA: K.McGuire, Private Communication.

d) TFR: Ref. [11]

e) JIPP-T-IIU: Shot No. 13316, 13318 (May 9 '84).

f) DITE: G.M.McCracken, Private Communication.

TABLE I. Current Termination Time on Several Tokamaks

These numbers are obtained from Ref. [17] .

κ means plasma elongation.

Device	τ_{mq} (ms)	Ip (MA)	R (m)	a (m) $<\kappa>$	$\sqrt{\kappa a^2 R I_p}$
JET	30	2.4	2.96	1.05 $<1.2>$	3.1
TFTR	10	1.0	2.5	0.8	1.3
PLT	1.2	0.35	1.3	0.4	0.27
PDX	1.0	0.3	1.4	0.4	0.26
D-III	10 3	1.5 0.3	1.45	0.4 $<1.3>$	0.67 0.30
ISX-B	1	0.1	0.93	0.27	0.082
Alcator-A	0.8	0.2	0.54	0.09	0.030
Alcator-C	1	0.45	0.64	0.17	0.09
T-10	5	0.2	1.5	0.4	0.22
TOSCA	0.05	0.02	0.3	0.08	0.0062
TFR	4	0.4	0.98	0.2	0.13
JIPP T-IIU	2.0	0.25	0.91	0.23	0.12
DIII-E	4	0.12	1.17	0.26	0.10

FIGURE CAPTIONS

Fig.1 Wall power loss during NBI heating on PDX.
(a) Giant sawtooth discharge with 2 beams (3.5 MW)
(b) Fishbone discharge with 4 beams (6.6 MW)
Pyroelectric signals P_{pyro} are compared with off-axis soft-X-ray intensity, central ECE temperature and Mirnov signals.
These pyro signals could not follow some fishbone peaks, because of the use of the slow (0.5 ms sampling) A-D convertor.

Fig.2 Total radiation power loss P_{rad} obtained by the thermistor array, and the ratio of time-averaged pyro signal $\bar{P}_{pyro}$ and fluctuation level $\tilde{P}_{pyro}$ related to beam-induced giant-sawteeth and fishbone oscillations, as a function of beam heating power P_{beam}.

Fig.3 Typical disruption characteristics in PDX.
At t = 462 ms the minor disruption occurs and is followed with the major disruption at t = 467 ms.

Fig.4 Schematic model for plasma behavior during major disruptions.

Fig.5 Scaling for current quench period of the disruption given by Eq.(13).
Typical experimental data from several tokamaks are plotted.
(See TABLE I.)

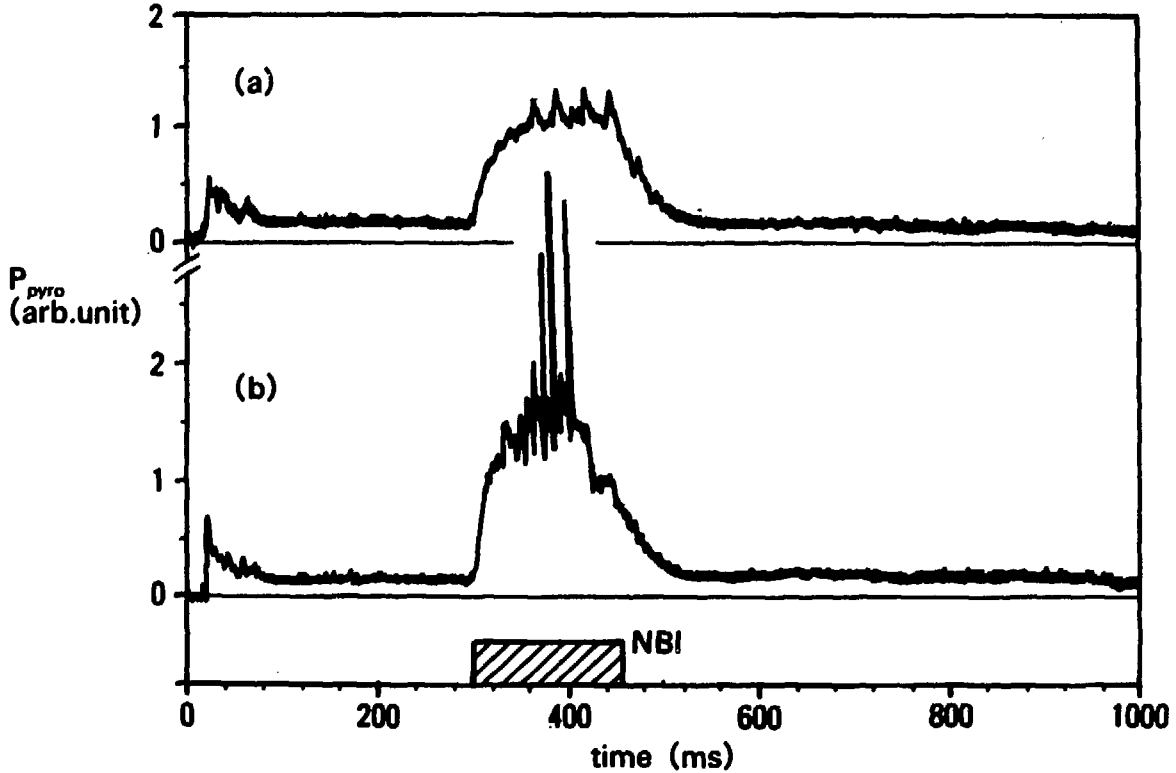

Fig. 1 (continues)

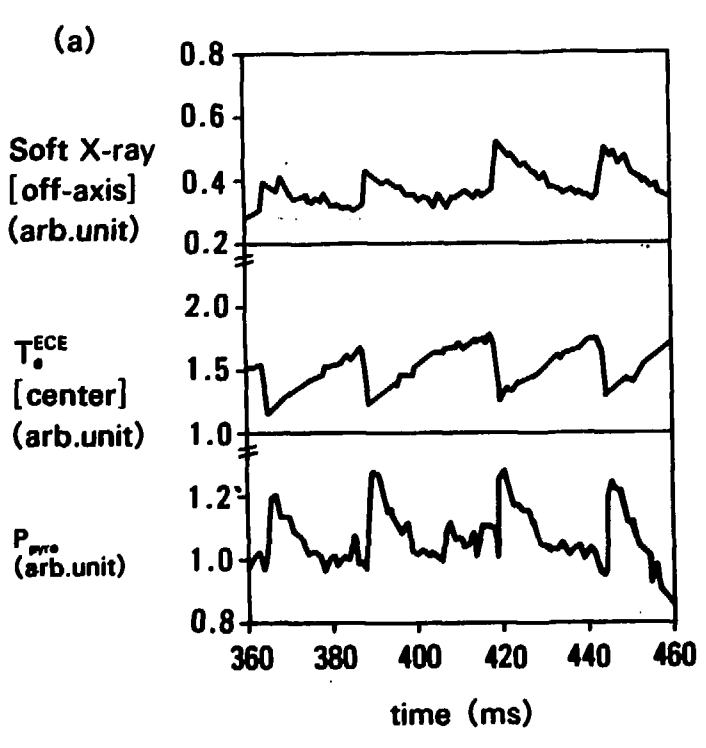

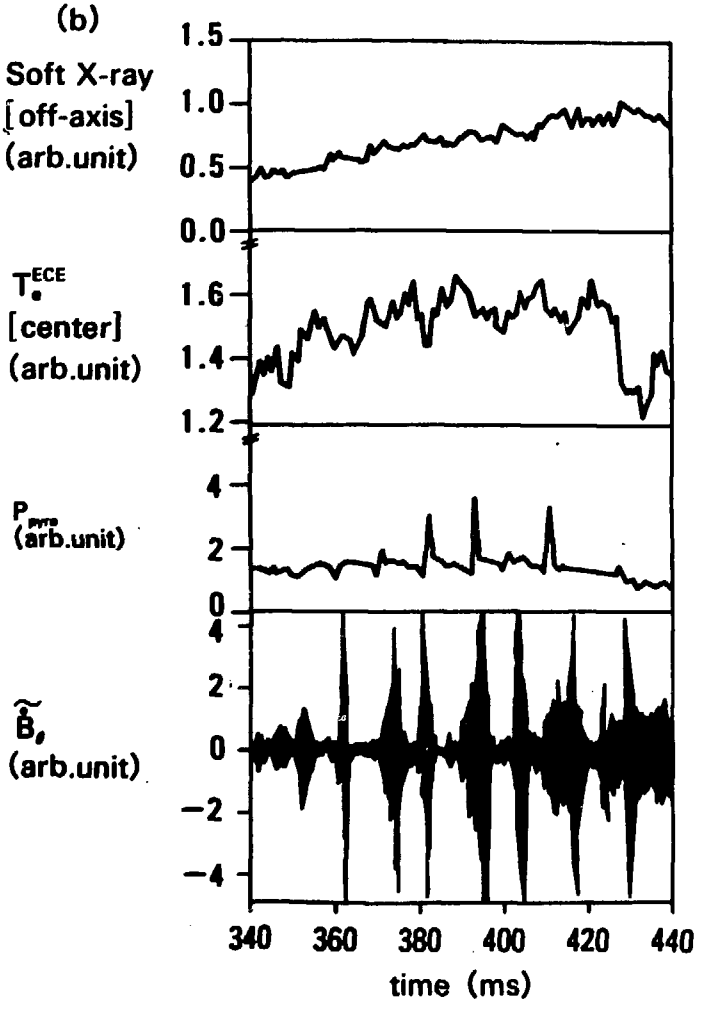

Fig. 1 (continued)

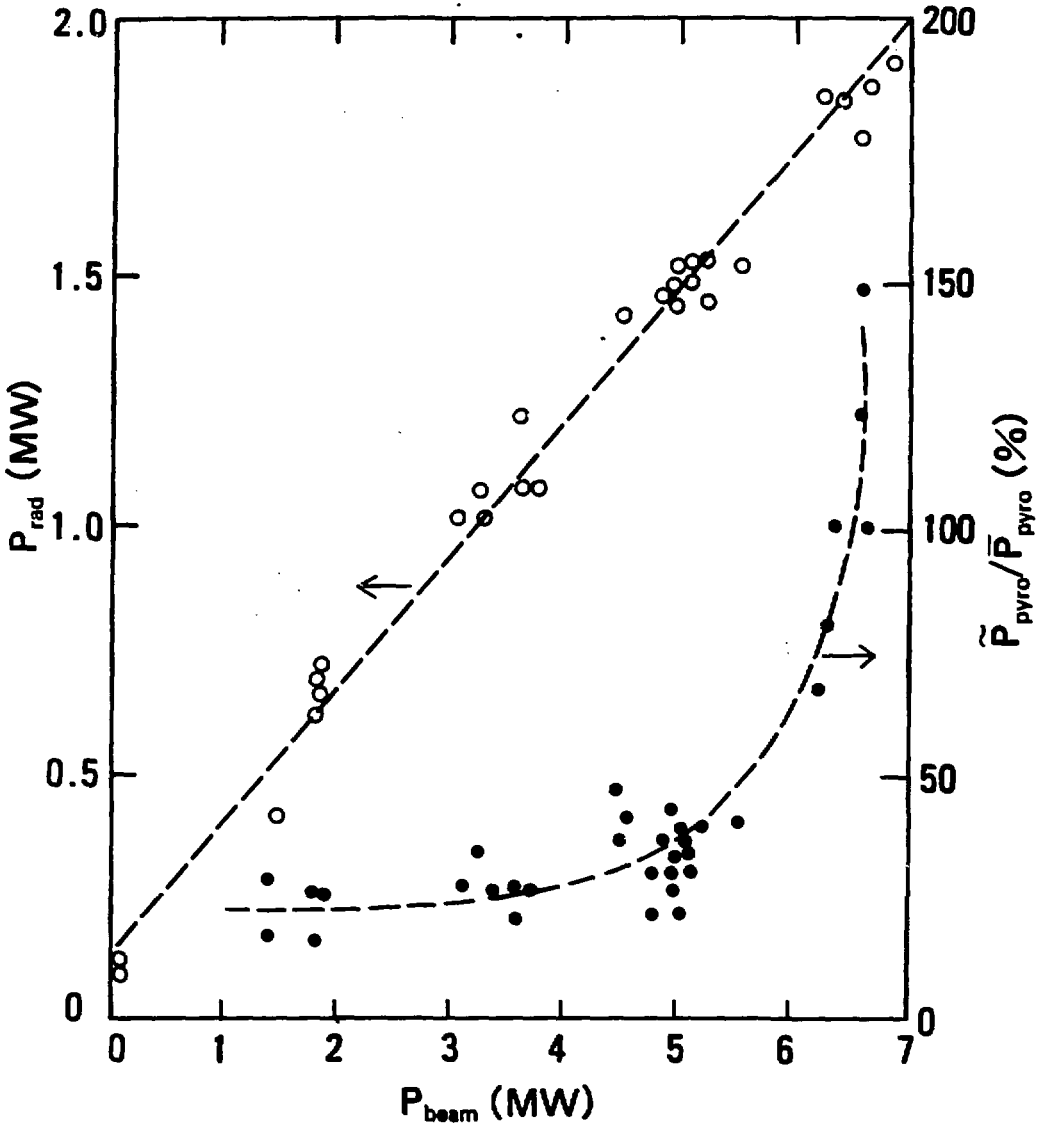
2.0
1.5
1.0
0.5
0
200
150
100
50
0
0
1
2
3
4
5
6
7
P_{rad} (MW)
P_{beam} (MW)
$\tilde{P}_{pyro}/\bar{P}_{pyro}$ (%)

Fig. 2

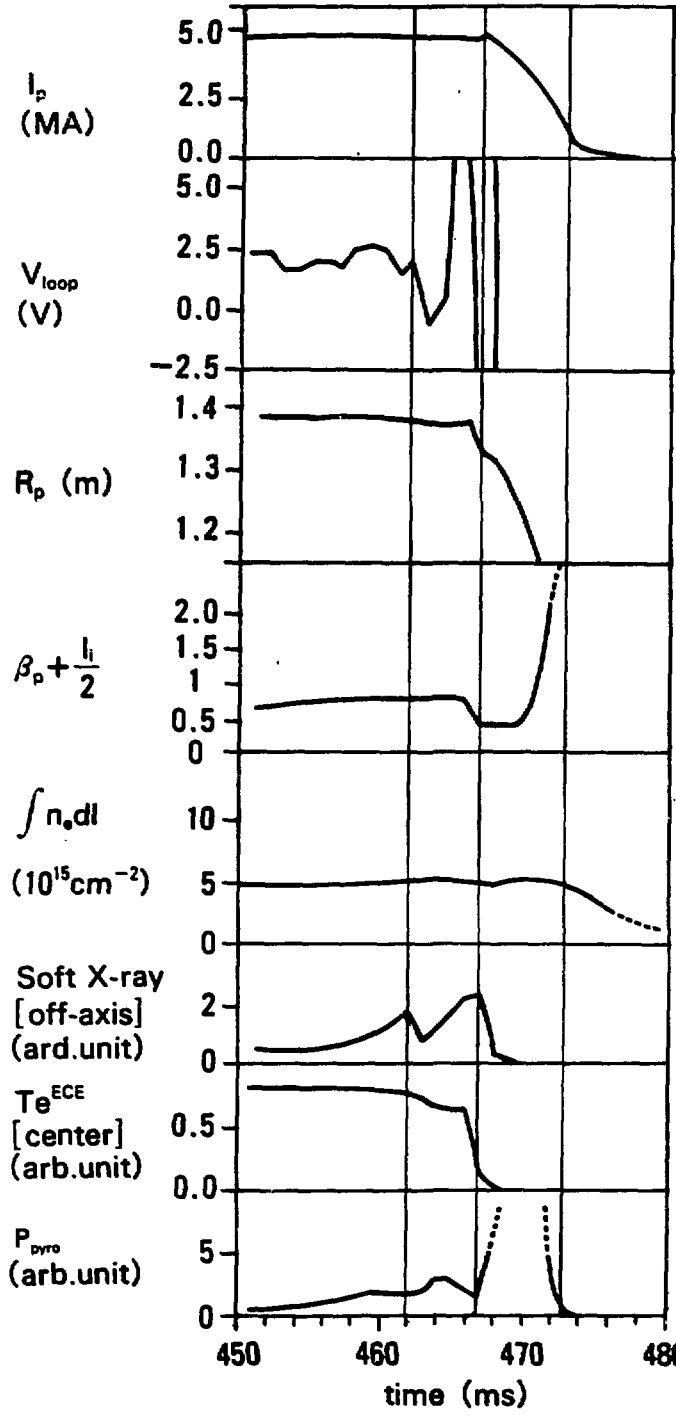
I_p (MA)
5.0
2.5
0.0
V_{loop} (V)
5.0
2.5
0.0
−2.5
R_p (m)
1.4
1.3
1.2
$\beta_p + \frac{l_i}{2}$
2.0
1.5
1
0.5
0
$\int n_e dl$ ($10^{15}cm^{-2}$)
10
5
0
Soft X-ray [off-axis] (ard.unit)
2
0
Te^{ECE} [center] (arb.unit)
0.5
0.0
P_{pyro} (arb.unit)
5
0
450
460
470
480
time (ms)

Fig. 3

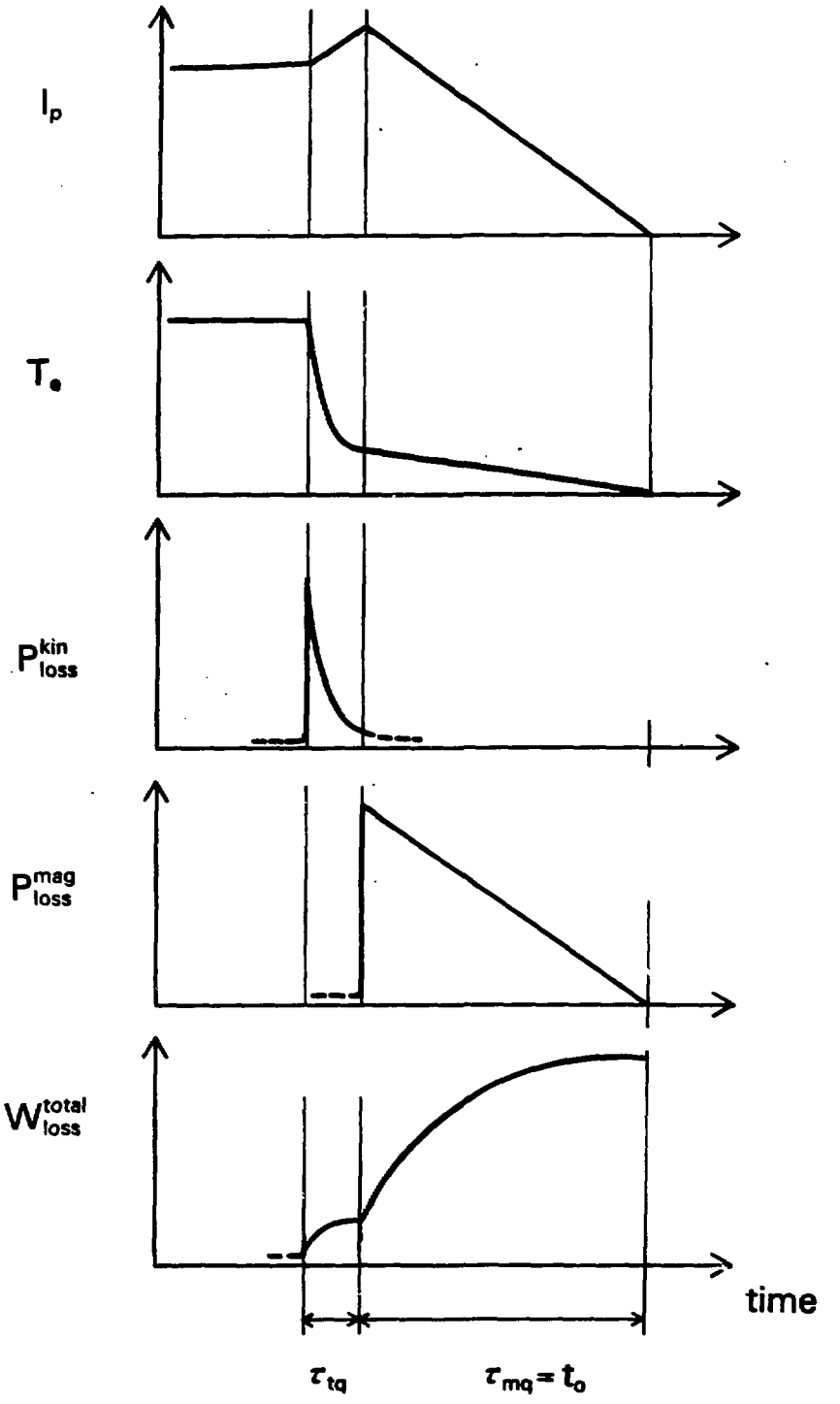

Fig. 4

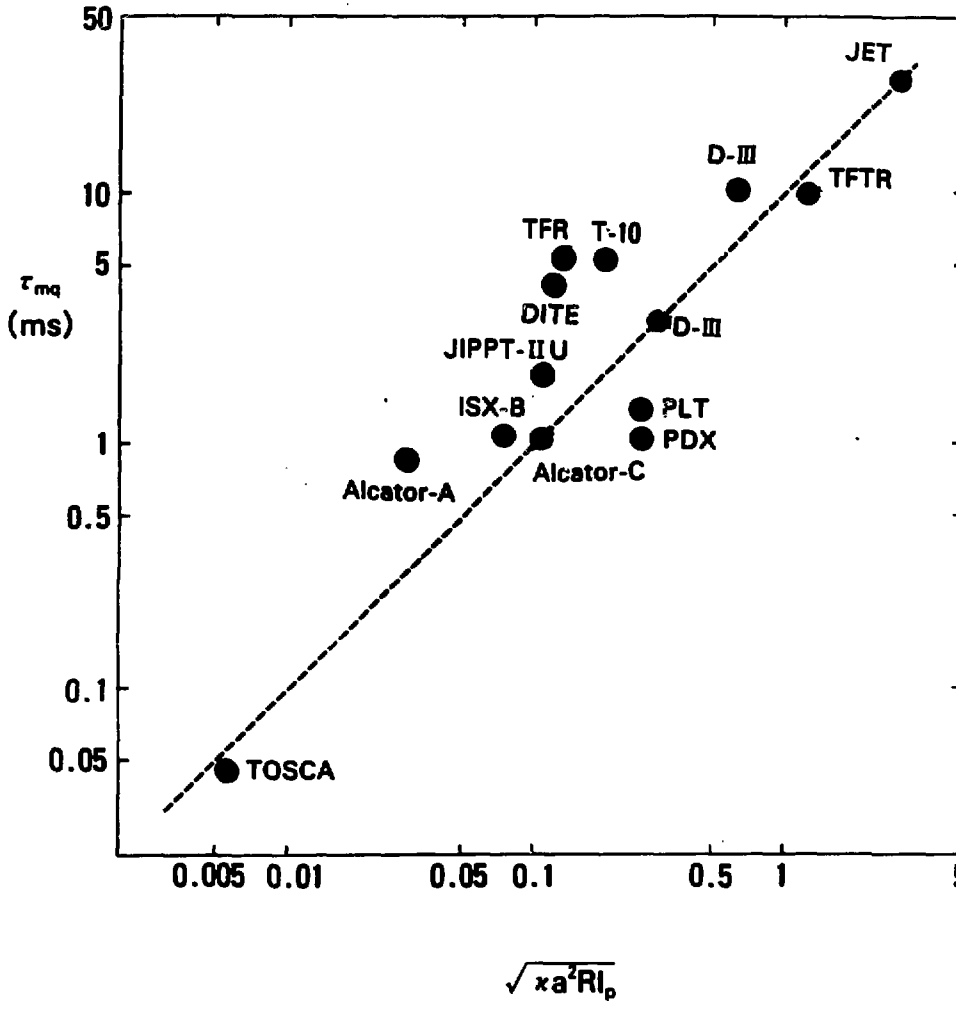
50
10
5
1
0.5
0.1
0.05
τ_{mq}
(ms)
JET
D-III
TFTR
TFR
T-10
DITE
D-III
JIPPT-IIU
ISX-B
PLT
PDX
Alcator-C
Alcator-A
TOSCA
0.005
0.01
0.05
0.1
0.5
1
5
$\sqrt{\kappa a^2 R I_p}$

Fig. 5